PROCEEDINGS OF SCIENCE

Absolute calibration and investigation of ageing of the AERA radio detectors

R. M. de Almeida[a,*] **for the Pierre Auger Collaboration**[b,†]

[a] *Universidade Federal Fluminense,*
Av. dos Trabalhadores 424, Volta Redonda, Brazil
[b] *Observatorio Pierre Auger, Av. San Martín Norte 304, 5613 Malargüe, Argentina.*

E-mail: rmenezes@id.uff.br, spokespersons@auger.org

The Auger Engineering Radio Array (AERA) is currently the largest facility to measure radio emissions from extensive air showers. Located at the Pierre Auger Observatory in Argentina, it comprises 153 autonomous radio-detector stations, covering an area of 17 km^2, and measures radio waves in the frequency range from 30 to 80 MHz. For the correct interpretation of data collected by AERA stations, the detector response has to be carefully calibrated. In the past, this was done by measuring the analogue chain in the laboratory, in addition to simulating and measuring the directional response of the antenna. In this work, we perform an absolute calibration by using the radio emission from the Galaxy. A model of the full radio sky is propagated through the system response, including the antenna, filters and amplifiers, and compared to the average spectra recorded by the stations. The method to determine the calibration constants, as the results, for each antenna will be presented. The behavior of the calibration constants is studied as a function of time from 2014 to 2020. There is no relevant ageing effect over a timescale of 10 years, showing that radio detectors could help to monitor possible ageing effects of other detector systems during long-term operations, stressing their importance in determining an absolute energy scale.

9th International Workshop on Acoustic and Radio EeV Neutrino Detection Activities - ARENA2022
7-10 June 2022
Santiago de Compostela, Spain

*Speaker
†Full author list at http://www.auger.org/archive/authors_2022_06.html.

PoS(ARENA2022)039

1. Introduction

The Auger Engineering Radio Array (AERA) [1], part of the Pierre Auger Observatory [2], is currently the largest system designed to measure radio emissions from extensive air showers. It is composed of 153 autonomous Radio Detector Stations (RDS), covering an area of 17 km^2.

An accurate description of the detector response is necessary for the correct interpretation of the data collected by the stations. This has already been achieved by measuring the analogue chain in the laboratory, in addition to simulating and measuring the directional response of the antenna. In this work, we perform an absolute Galactic calibration of the RDS and investigate the behavior of the calibration constants as a function of time from 2014 until 2020. Being an engineering array, different types of antennas have been designed, installed and tested in the field. In this work, we use only Butterfly [3] stations, designed to measure radio emission in the frequency range between 30 MHz and 80 MHz in two polarization directions (east-west and north-south directions relative to magnetic north).

The paper is structured in the following way: section 2 presents the data set used in this study. The radio sky model used in this work is described in section 3 while the method applied to perform the absolute calibration is detailed in section 4. The calibration results are shown in section 5 and the study of calibration constants as a function of time is described in section 6. Finally, the conclusions are presented in section 7.

2. Data set

The data set used to perform the Galactic calibration consists of periodically triggered traces, sampled every 100 seconds, measured from 2014 until 2020. The traces are corrected for an observed anti-correlation between peak amplitude and temperature caused by temperature-dependent gain variations of amplifiers in the signal chain, which had been characterized previously from lab measurements. The power received by the antenna is given by

$$P_\nu = 2\frac{1}{T}\sum_{k=\nu}^{\nu+\delta}\frac{|V(k)|^2}{Z_L}\Delta\nu \tag{1}$$

where T is the length of the trace, $V(k)$ is the measured spectral voltage at frequency k, Z_L is the antenna impedance and $\Delta\nu$ is the frequency bin resolution. The periodic data give us a good measure of the Galactic background, but they may also contain cosmic-ray signals, radio-frequency interference (RFI) from external sources and internal electronic noise. RFIs can be divided into two classes: broadband and narrowband. Narrowband noise has as its main characteristic the continuous emission in the entire local sidereal time (LST) range and is produced by sources that continuously emit radio signals at specific frequencies. The most intense narrowband noises are produced by AERA beacons installed at the Auger site. These noises are so intense that it makes it difficult to reveal the transit of the Galactic center in the dynamic frequency spectrum. Therefore, these frequency bands are identified and removed from the data set with the corresponding gaps interpolated. On the other hand, broadband RFIs are transient radio pulses that are also sources of contamination in the data. To remove broadband noises and cosmic-ray signals, we implement a

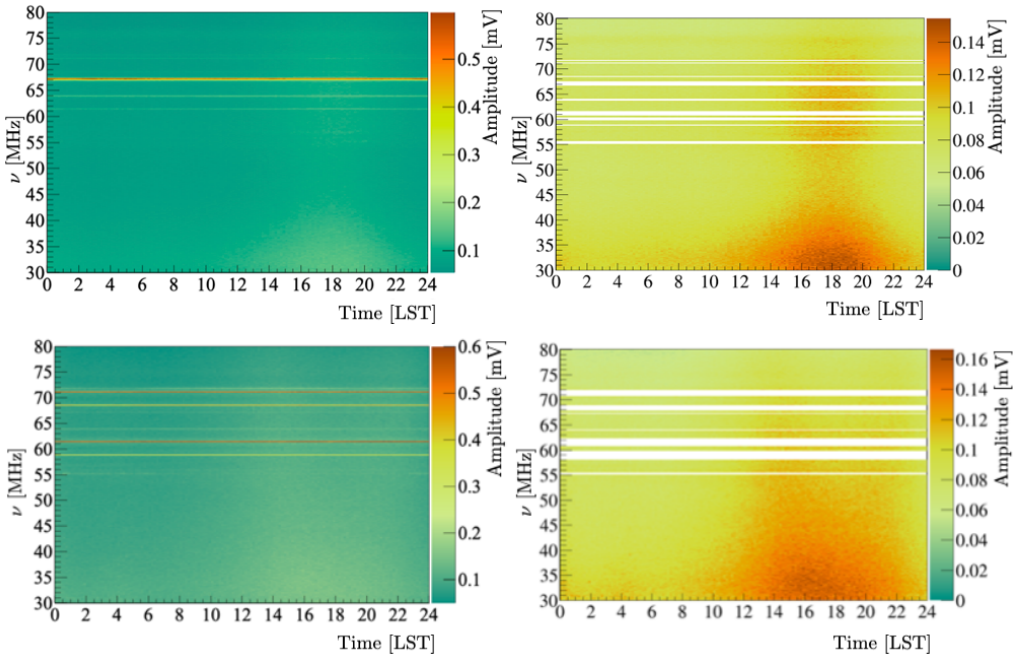

Figure 1: Dynamic average frequency spectrum as a function of LST for the east-west (top) and north-south (bottom) channel for antenna ID:53 for the period of February 2017. The left panels present the results before removal of narrowband RFI (horizontal lines) while the right ones show that the Galactic signal becomes evident after RFI removal.

time-dependent threshold in LST. For this, we obtain the average spectral density of each antenna according to

$$\langle I \rangle = \frac{1}{n}\sqrt{\sum_{i=1}^{n} A^2(\nu_i)}, \tag{2}$$

where $A(\nu_i)$ is the signal amplitude in frequency bin i, n is the total number of bins and t is the time bin in LST. For each LST time bin of 8 minutes, we performed a Gaussian fit $G(I;\bar{I},\sigma_I)$ on the collected average spectral densities. Average spectral densities greater than the threshold $I^{\rm th}_{\rm LST}$ defined as $\int_{-\infty}^{I^{\rm th}_{\rm LST}} G(I;\bar{I},\sigma_I) = 0.9973$ (equivalent 3σ) are removed from the data. This procedure is repeated on a monthly basis for all antennas and for both channels. As illustration, Fig.1 presents the dynamic average frequency spectrum before and after the RFI subtraction for both channels, showing that the Galactic modulation becomes evident after the noise is removed.

3. Radio sky model

The background radio signal received on Earth varies in different directions across the sky and can be conveniently specified by its equivalent brightness temperature $T_{\rm sky}$. For the frequency range of the AERA antennas (30 MHz - 80 MHz) the background signal is dominated by Galactic emission and the total expected power to be received by the antenna is calculated as

$$P_{\rm sky}(t,\nu) = \frac{Z_0}{Z_{\rm L}}\frac{k_{\rm B}}{c^2}\int_{\Omega} \nu^2 T_{\rm sky}(\nu,\alpha,\delta)|H_i(\nu,\alpha,\delta)|^2 d\Omega, \tag{3}$$

where k_B is the Boltzmann constant, c is the speed of light, Z_0 is the impedance of free space given by 120π Ω and Z_L is the antenna impedance. $H_i(\nu, \alpha, \delta)$ is the directional response of the antenna and T_{sky} is described as a combination of the cosmic microwave background CMB, an isotropic emission due to unresolved extra-galactic sources and an anisotropic Galactic emission that is provided by the LFmap software [4]. The simulated power P_{sky} in frequency bins of 1 MHz and LST bins of 1 hr is illustrated in Fig. 2. Besides the LFmap, there are different available models for the galactic emission [5–7]. An estimation of the systematic uncertainties on the prediction of the Galactic emission from sky models was obtained in [8].

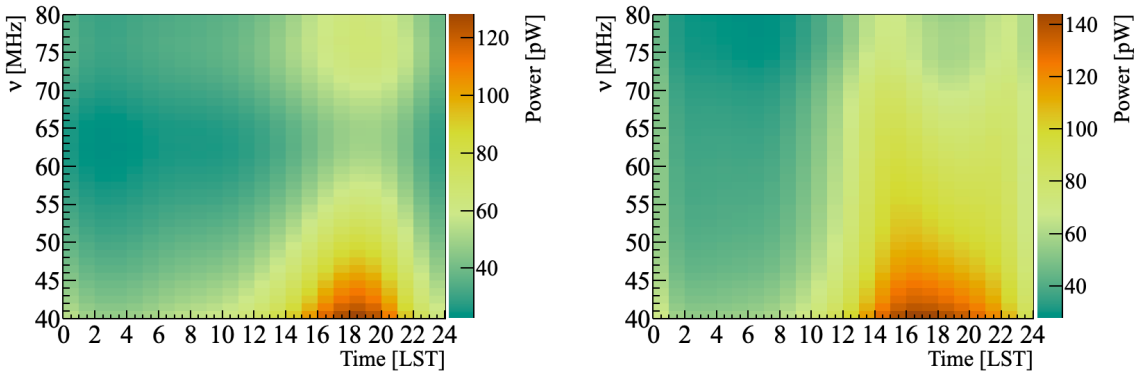

Figure 2: The left (right) panel shows the simulated power P_{sky} as a function of LST and frequency for the east-west (north-south) channel.

4. Calibration Method

For a correct interpretation of AERA data, accurate knowledge of the whole signal chain (antenna, amplifiers, filters and digitizer) is necessary to reduce measurement uncertainties. Therefore, the antennas must be carefully calibrated. For this, an approach inspired by the calibration technique used in the LOFAR experiment [9] was used, where we take into account the convolution of the power emitted by the sky with the gains and noises entering the antenna signal chain but also allowing for a possible external environmental noise. In this way, the power emitted by the sky and propagated by the antenna can be described by

$$P_{\text{model}}(t, \nu) = P_{\text{sky}}(t, \nu) G_{\text{ant}}(\nu) G_{\text{RCU}}(\nu) C_0^2(\nu) + N_{\text{tot}}(\nu), \tag{4}$$

in which $G_{\text{ant}}(\nu)$ and $G_{\text{RCU}}(\nu)$ are, respectively, the gains of the Low Noise Amplifier (LNA) and of the receiver unit (RCU), where the signal is subjected to a bandpass filter, amplified and digitized. Besides, $C_0(\nu)$ is the calibration constant and the total noise $N_{\text{tot}}(\nu)$ is a sum of the intrinsic electronic thermal noise and the environmental one.

The calibration is therefore performed by comparing the actual signal recorded in the antenna with the expected signal from Eq. 4 so that a linear fit for each frequency band provides the values of $C_0^2(\nu)$ and $N_{\text{tot}}(\nu)$.

5. Calibration Results

The fit procedure was done only for frequency bands above 40 MHz, since the range between 30 MHz and 40 MHz was removed from the data due to a large amount of noise. As illustration, Fig. 3 shows the results of the linear fit in each frequency band for the antenna Id: 33 for the east-west channel. The angular and linear coefficients obtained in each fit represent the calibration constant squared $C_0^2(\nu)$ and the total noise $N_{\rm tot}(\nu)$, respectively.

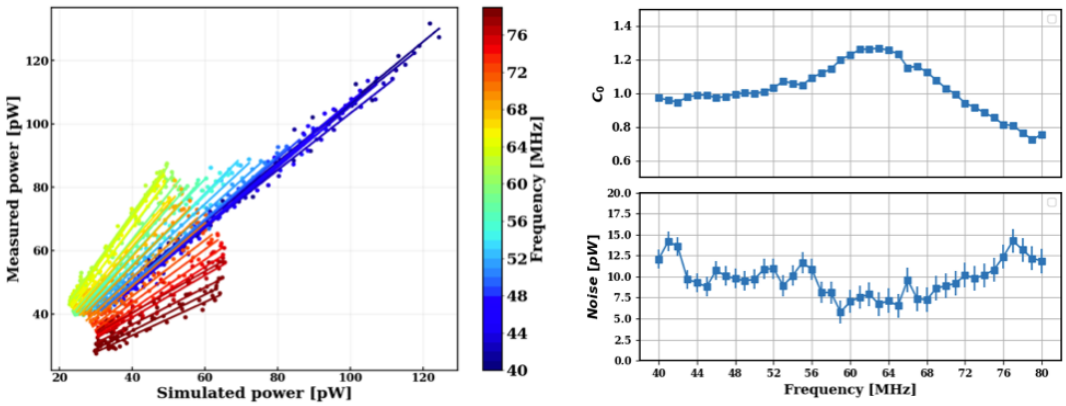

Figure 3: Calibration result for antenna Id:33 on east west channel for the period 2017/02. Left: linear fit produced for each frequency band. Right: Calibration constant C_0 and noise for each frequency band.

Due to the asymmetry in the antenna directional response and the presence of different noise measured in different polarizations produced by man-made noise sources, the calibration constants are computed for each antenna and channel as a function of frequency. The fit was performed on a monthly basis, totaling 84 months. Within this period, 52 of the Butterfly antennas were in operation and were used in this study. Figure 4 shows the averages and RMS of the calibration constants and noises per frequency obtained for both channels considering all antennas during the entire period considered. The strong deviation between ~55 MHz and ~70 MHz in the east-west channel results from a not perfect description of the antenna directional response, probably related to the effect of the electronic box.

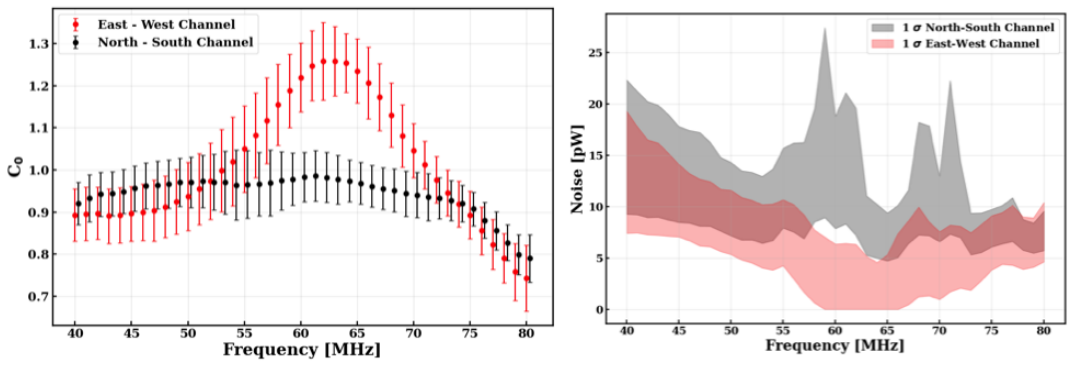

Figure 4: Results obtained by all antennas in the period from 2014 / 01 to 2020 / 12 for both channels. Left: calibration constants as a function of frequency. Right: total noise per frequency. The bands correspond to 1σ interval of the distribution.

6. Study of the calibration constant as a function of time

In this section, we study the behavior of the calibration constants as a function of time. The calibration constant C_0 for each antenna channel, computed on a monthly basis, is considered to be the average of the calibration constants as a function of frequency $\langle C_0(\nu)\rangle$. Therefore, considering a linear fit $C_0(t) = at + b$, with t given in months since the beginning of 2014, the slope parameter a can be interpreted in terms of ageing per month. As an illustration of the method, Figure 5 shows the behavior of the calibration constants for both channels of antenna Id:33 from 2014 until the end of 2020. A remaining seasonal modulation is observed, possibly related to a larger moisture of the ground on the Southern Hemisphere Summer in relation to Winter. Despite that, a linear fit, represented by the red line, is performed.

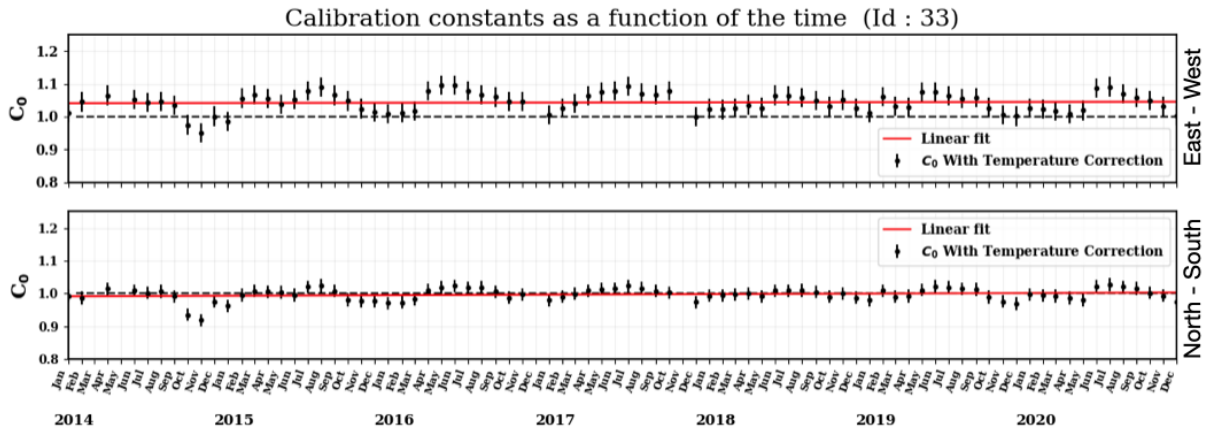

Figure 5: Calibration constants obtained for both channels of antenna Id:33 from 2014 to 2020. The corresponding linear fit is represented by the red line.

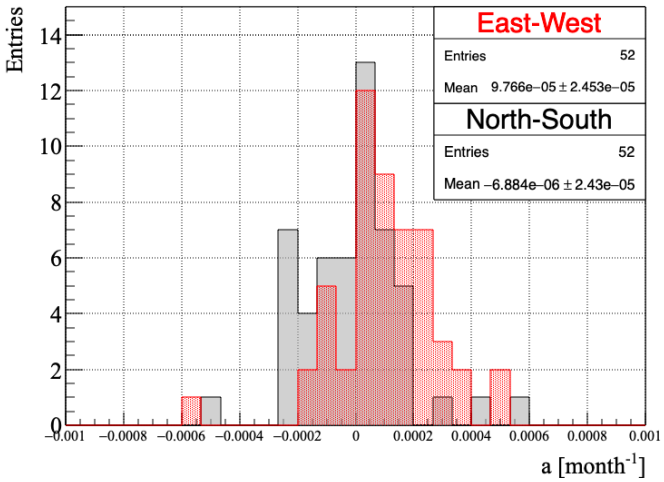

Figure 6: Distribution of the angular coefficients a, interpreted as the ageing factor per month, obtained from each antenna and channel.

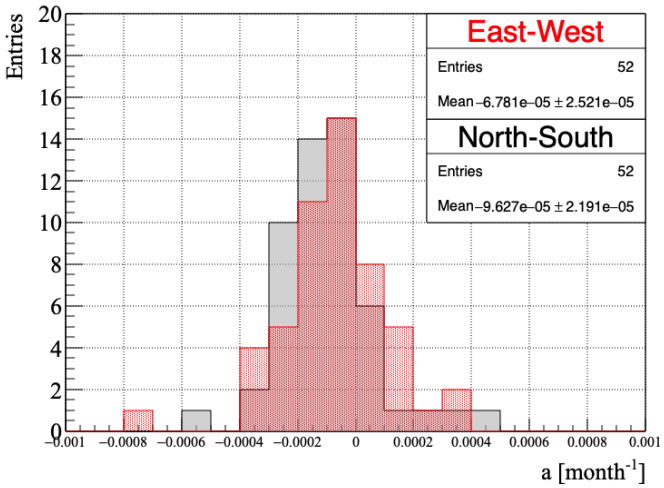

Figure 7: Distribution of the angular coefficients a, interpreted as the ageing factor per month, obtained from each antenna and channel, after removing the measurements corresponding to November and December of 2014.

We repeated this procedure for all 52 butterfly antennas. The distribution of the fitted coefficients a is shown in Fig. 6 where one can see that it is reasonably centered at zero. The values of the fitted parameters a correspond to an ageing factor of (1.17 ± 0.29)% per decade for the east-west channel and of (-0.08 ± 0.26)% per decade for the north-south channel. The small positive value for the east-west channel seems to be a result of a strong downward fluctuation observed for several antennas in November and December 2014. Discarding such points from the fit would result in the distribution shown in Figure 7. Notice that the distributions are more centered at zero, with negligible mean values for a of (-0.80 ± 0.30)% and (-1.10 ± 0.26)% per decade for channels east-west and north-south, respectively.

7. Conclusions

In this work, we performed an absolute Galactic calibration of AERA stations. The calibration constants obtained are close to 1, indicating a good agreement with the original calibration, performed by measuring the analogue chain in the laboratory and simulating the directional response of the antenna. Besides, we studied the behavior of the calibration constants as a function of time from 2014 to 2020, and we show that there is no relevant ageing effect for the AERA stations. The results show that radio detectors can help monitor ageing effects observed in other detectors that operate over long time periods, especially important in the context of the Pierre Auger Observatory upgrade [10], and emphasizes the importance of the radio detection technique for determining an absolute energy scale for cosmic rays.

References

[1] P. Abreu, M. Aglietta, M. Ahlers, E. Ahn, I.F.d.M. Albuquerque, D. Allard et al., *Antennas for the detection of radio emission pulses from cosmic-ray induced air showers at the Pierre Auger Observatory*, *Journal of Instrumentation* **7** (2012) P10011.

[2] Pierre Auger Collaboration et al., *The Pierre Auger cosmic ray observatory*, *Nuclear Instruments and Methods in Physics Research Section A: Accelerators, Spectrometers, Detectors and Associated Equipment* **798** (2015) 172.

[3] D. Charrier and Codalema Collaboration, *Antenna development for astroparticle and radioastronomy experiments*, *Nuclear Instruments and Methods in Physics Research Section A: Accelerators, Spectrometers, Detectors and Associated Equipment* **662** (2012) S142.

[4] E. Polisensky, *Lfmap: A low frequency sky map generating program*, *Long Wavelength Array Memo Series* **111** (2007) 515.

[5] A. De Oliveira-Costa, M. Tegmark, B.M. Gaensler, J. Jonas, T.L. Landecker and P. Reich, *A model of diffuse Galactic radio emission from 10 MHz to 100 GHz*, *Monthly Notices of the Royal Astronomical Society* **388** (2008) 247.

[6] H. Zheng, M. Tegmark, J.S. Dillon, D.A. Kim, A. Liu, A.R. Neben et al., *An improved model of diffuse galactic radio emission from 10 MHz to 5 THz*, *Monthly Notices of the Royal Astronomical Society* **464** (2016) 3486.

[7] J. Dowell, G.B. Taylor, F.K. Schinzel, N.E. Kassim and K. Stovall, *The LWA1 Low Frequency Sky Survey*, *Monthly Notices of the Royal Astronomical Society* **469** (2017) 4537.

[8] M. Büsken, T. Fodran and T. Huege, *Uncertainties of the 30-408 MHz galactic emission as a calibration source for radio detectors in astroparticle physics*, *arXiv preprint arXiv:2211.03086* (2022) .

[9] K. Mulrey, A. Bonardi, S. Buitink, A. Corstanje, H. Falcke, B. Hare et al., *Calibration of the LOFAR low-band antennas using the galaxy and a model of the signal chain*, *Astroparticle physics* **111** (2019) 1.

[10] A. Aab, P. Abreu, M. Aglietta, E. Ahn, I.A. Samarai, I. Albuquerque et al., *The Pierre Auger Observatory upgrade-preliminary design report*, *arXiv preprint arXiv:1604.03637* (2016) .

PoS(ARENA2022)039